APPLIED AND ENVIRONMENTAL MICROBIOLOGY, Dec. 2005, p. 8773–8783 Vol. 71, No. 12
0099-2240/05/$08.00+0 doi:10.1128/AEM.71.12.8773–8783.2005
Copyright © 2005, American Society for Microbiology. All Rights Reserved.

Desulfotomaculum and *Methanobacterium* spp. Dominate a 4- to 5-Kilometer-Deep Fault

Duane P. Moser,[1]* Thomas M. Gihring,[1]† Fred J. Brockman,[1] James K. Fredrickson,[1] David L. Balkwill,[2] Michael E. Dollhopf,[2]‡ Barbara Sherwood Lollar,[3] Lisa M. Pratt,[4] Erik Boice,[4] Gordon Southam,[5] Greg Wanger,[5] Brett J. Baker,[6] Susan M. Pfiffner,[7] Li-Hung Lin,[8]§ and T. C. Onstott[8]

Environmental Microbiology Group, Pacific Northwest National Laboratory, Richland, Washington 99352[1]; Department of Biomedical Sciences Biology, The Florida State University, Tallahassee, Florida 32306[2]; Department of Geosciences, University of Toronto, Toronto, Ontario M5S 3B1, Canada[3]; Department of Geological Sciences, Biogeochemical Laboratories, Indiana University, Bloomington, Indiana 47405[4]; Department of Earth Sciences, University of Western Ontario, London, Ontario N6A 5B7, Canada[5]; Earth and Planetary Sciences, University of California, Berkeley, California 94720[6]; Center of Biomarker Analysis, University of Tennessee, Knoxville, Tennessee 37932[7]; and Department of Geological and Geophysical Sciences, Princeton University, Princeton, New Jersey 08544[8]

Received 6 April 2005/Accepted 15 August 2005

Alkaline, sulfidic, 54 to 60°C, 4 to 53 million-year-old meteoric water emanating from a borehole intersecting quartzite-hosted fractures >3.3 km beneath the surface supported a microbial community dominated by a bacterial species affiliated with *Desulfotomaculum* spp. and an archaeal species related to *Methanobacterium* spp. The geochemical homogeneity over the 650-m length of the borehole, the lack of dividing cells, and the absence of these microorganisms in mine service water support an indigenous origin for the microbial community. The coexistence of these two microorganisms is consistent with a limiting flux of inorganic carbon and SO_4^{2-} in the presence of high pH, high concentrations of H_2 and CH_4, and minimal free energy for autotrophic methanogenesis. Sulfide isotopic compositions were highly enriched, consistent with microbial SO_4^{2-} reduction under hydrologic isolation. An analogous microbial couple and similar abiogenic gas chemistry have been reported recently for hydrothermal carbonate vents of the Lost City near the Mid-Atlantic Ridge (D. S. Kelly et al., Science 307:1428-1434, 2005), suggesting that these features may be common to deep subsurface habitats (continental and marine) bearing this geochemical signature. The geochemical setting and microbial communities described here are notably different from microbial ecosystems reported for shallower continental subsurface environments.

Numerous studies have revealed the presence of microbial communities occupying oceanic and terrestrial deep subsurface settings (12, 14, 23, 27, 53, 54). Due to its enormous volume, this habitat may host the majority of Earth's prokaryotes (76), and according to some estimates (25, 76), the collective biomass of subsurface microbiota may rival that of flora and fauna at the surface. It is generally accepted that life on Earth requires liquid water (9). The upper 4 km of the terrestrial crust contains 9.5×10^6 km^3 of groundwater, of which about 56% lies below 0.75 km in depth (6). Since reports of microorganisms over this depth interval continue (4, 53, 54, 70) and the basic requirements for life appear to be met (e.g., liquid water, habitable space, and permissive temperatures), it follows that a significant proportion of the biosphere may be microbial and associated with deep terrestrial hydrologic systems (76).

Although a reasonable understanding of the energetic foundations for marine and terrestrial subsurface sedimentary ecosystems to a depth of 500 m has been achieved (20, 55), mechanisms for the energetic support of igneous and metamorphic rock systems remain incompletely addressed. Best known are igneous rock-hosted aquifers at depths of <450 m, where chemolithoautotrophic subsurface ecosystems, founded upon biological methanogenesis or acetogenesis and supported by geological H_2 production and inorganic C, are thought to be limited in photosynthetically derived organic C (12, 56, 68). Relatively little is known, however, about the distribution of such communities at much greater depths or whether microbial ecosystems of other deep rock types (e.g., sedimentary and metamorphic) operate with similar energy and C sources.

Microbiological sampling opportunities in the deep subsurface are extremely limited, and a persistent challenge remains the differentiation of indigenous from introduced microorganisms (52). Several studies, however, have shown that in mine boreholes, introduced microbes fail to persist (47, 57), especially when the unidirectional flushing of hot, anaerobic fracture water reestablishes a redox environment similar to that of the predrilling conditions (47). South African mines are unusual in that they routinely attain depths of >3 kilometers below land surface (kmbls), thereby accessing thermophilic, anaerobic environments distinct from more frequently studied,

* Corresponding author. Present address: Desert Research Institute, 755 Flamingo Rd., Las Vegas, NV 89119. Phone: (702) 862-5534. Fax: (702) 862-5360. E-mail: duane.moser@dri.edu.

† Present address: Florida State University, Department of Oceanography, Tallahassee, FL 32306.

‡ Present address: Department of Civil and Environmental Engineering, Marquette University, P.O. Box 1881, Milwaukee, WI 53201.

§ Present address: Institute of Zoology, National Taiwan University, No. 1, Sec. 4, Roosevelt Road, Taipei 106, Taiwan.

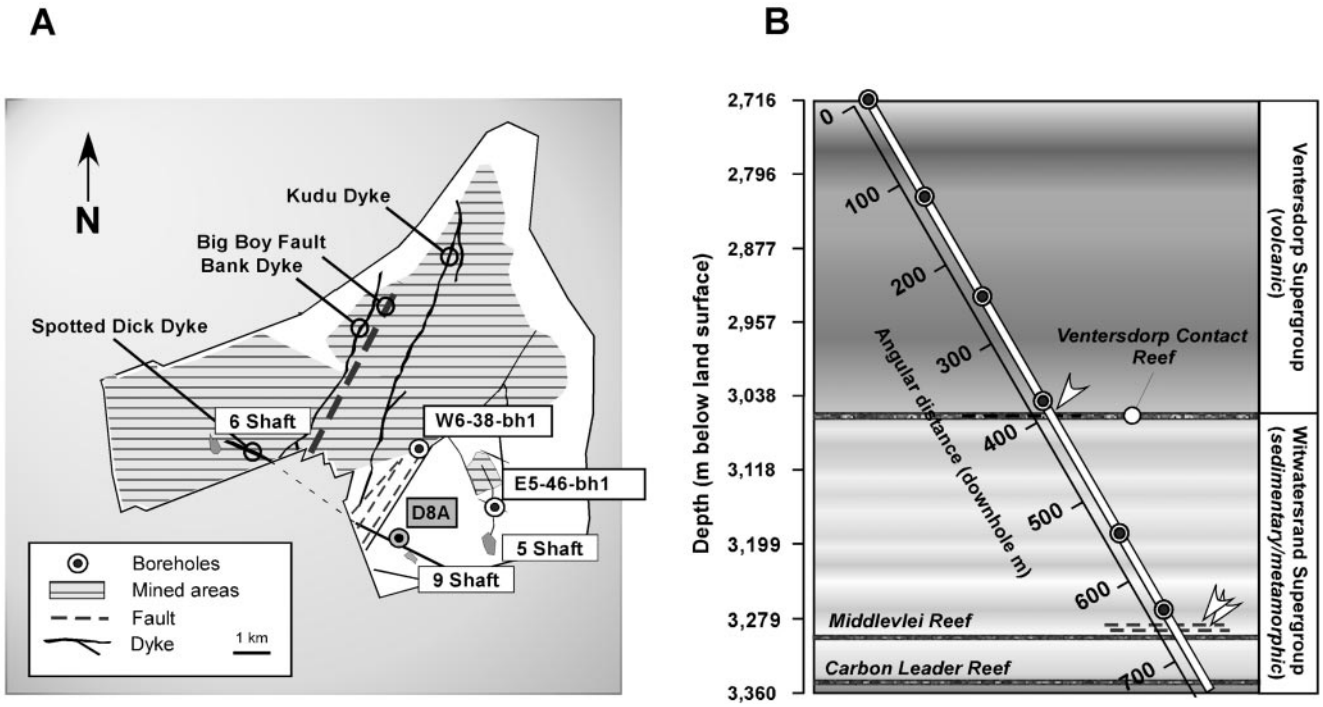

FIG. 1. (A) Plan view showing location of borehole D8A. The Driefontein property is outlined, and major geological features are labeled. Mined areas are hatched. The locations of the comparative boreholes mentioned in the text, W6-38-bh1 (4) and E5-46-bh1 (47), are shown. (B) Geological cross section intersected by borehole. The depth, in meters below the surface, is depicted along the vertical axis, and the angular downhole distance is also shown. Faults reported are denoted with arrowheads and dashed lines. Sampling intervals are denoted by circles.

shallower subsurface aquifers (56, 68). Mine drilling programs occasionally intersect pressurized fluid-filled fracture systems, some of which flush for years at rates of liters min^{-1}. Once purged of drilling-associated microbial and chemical contamination, flowing boreholes can be viewed as artificial artesian fractures and functional conduits into native deep subsurface habitats.

Here we describe such an artesian borehole, which being situated >1.5 km from the nearest current or historical mining activity, enabled the sampling of minimally impacted strata. Originating at 2.716 kmbls and extending downwards to 3.360 kmbls, the borehole intersected three faults. The borehole was uncased from 10 m below the outlet and had continuously flowed over the 12 months following drilling, producing $>2.8 \times 10^6$ liters (~2,400 borehole volumes) of 54°C, anaerobic water. Using a bailer, a profile of the fluid chemistry and microbial community structure was obtained from source faults deep within the borehole to the outlet.

MATERIALS AND METHODS

Site description. Driefontein Consolidated Mine (Fig. 1A) is located 70 km west of Johannesburg, South Africa, in the Carletonville mining region. The exploration borehole utilized here (D8A, Fig. 1B) was drilled into the floor of a horizontal tunnel about 700 m from the vertical access shaft (9 Shaft). The mine transects an Archean-aged stratigraphic section typical of the western Witwatersrand Basin (62). The 2.5 billion-year (Ga) Pretoria and Chuniespoort groups, with the latter hosting a dolomite aquifer, extend to about 2 kmbls. Below them lies the metabasaltic, 2.7-Ga Ventersdorp supergroup, which in turn overlies the 2.9-Ga Witwatersrand supergroup quartzite. At the Witwatersrand/Ventersdorp boundary is a commercial Au deposit, the Ventersdorp Contact Reef (VCR), and within the Witwatersrand supergroup are two additional ore zones, the Middelvlei and Carbon Leader reefs (Fig. 1B). In the Carletonville mining district, water below the dolomite is confined to fractures and ranges in age from 4 to 165 million years (Ma) (41).

Borehole D8A was drilled 60° from horizontal to a length of 743 m (644 m vertical, Fig. 1B). The upper 10 m was steel cased (80-mm internal diameter), and the remainder (50-mm internal diameter) was uncased. The outlet (2.716 kmbls) was located within the Ventersdorp supergroup; the VCR was intersected at 400 m (3.058 kmbls), and the Carbon Leader reef was intersected at 720 m (3.340 kmbls). In the corresponding core, faults were recorded within the VCR, at 650 and 670 m (3.28 and 3.30 kmbls). Drilling was completed in October 2000, and sampling was conducted from August to November 2001. Flowing water was noted upon the completion of coring, and water and gas production rates of 4.5 and 4.6 liters min^{-1}, respectively, were measured on 7 November 2001.

Sampling. The outlet sample was collected with an expandable steel packer (Cementation Engineers, Johannesburg, South Africa) customized with a nylon insert to eliminate metal-water contact. Water and gas samples were collected anaerobically using a Delrin plastic (DuPont) valved manifold (46). To obtain samples from depth, a chlorine bleach-disinfected bailer was deployed with a wire winch. The bailer was tested to 100 m using sterile rhodamine WT (1,000 mg $liter^{-1}$) as a tracer. Upon retrieval, gas accumulated below the upper ball valve, which was subsampled via a dedicated sampling port with a gas-tight syringe. Water samples for microbiological and geochemical analyses were collected anaerobically from the bottom of the bailer.

Filtered (0.22-μm nylon Acrodisk; Gelman) samples included anions, cations, and NH_3, preserved as described previously (47). Bottles for unfiltered samples were preloaded with preservatives and capped without headspace. These included dissolved inorganic carbon (DIC) and [δ^{13}C]DIC (140-ml serum vials with 200 μl of saturated $HgCl_2$), NH_3 (140-ml serum vials with 50 μl concentrated H_2SO_4), HS^- (20-ml glass serum vials with 500 μl 2 M Zn acetate), δ^{34}S (60-ml plastic syringes with 500 μl 2 N Zn acetate), δ^2H and δ^{18}O (140-ml and 20-ml serum vials), dissolved gases (140-ml evacuated serum vials with 200 μl of saturated $HgCl_2$), organic acids (45-ml serum vials), dissolved organic carbon (DOC) and total organic carbon (TOC) (45-ml glass vials with Teflon septa containing 2 ml concentrated HCl), and HPO_4^{2-} (acid-washed 250-ml Nalgene bottles). The anion, HPO_4^{2-}, and organic acid sample bottles were partially filled and frozen. The δ^{34}S samples were refrigerated. Due to volume limitations,

TABLE 1. Major anions and cations in borehole D8A

Depth (m)—date (mo/day/yr)	Temp (°C)	Concn (mM) of indicated species[a]												
		TOC	Acetate	Formate	Propionate	DIC	Cl^-	HS^-[b]	SO_4^{2-}	NH_4^+	Na^+	Ca^{2+}	Mg^{2+}	Fe^{2+}
Outlet—08/30/01	43.3	0.29	0.013	0.0005	0.0002	0.104	31.0	0.60 (0.494)	0.125	0.011	13.9	1.7	0.027	0.0013
Outlet—09/15/01	43.3	NA	NA	NA	NA	NA	NA	NA	NA	0.006	14.5	1.9	<0.002	<0.0001
Outlet—10/24/01	43	0.40	0.035	0.0020	0.0007	0.104	31.7	1.48	0.137	<0.011	11.1	1.7	0.006	0.00002[c]
125—10/24/01	46	0.11	0.033	0.0020	0.0007	0.139	26.3	0.60	0.033	<0.011	15.5	2.3	0.010	0.0009[c]
125—10/25/01	46	NA	0.040	0.0041	0.0014	NA	25.9	NA	0.037	0.082	16.5	2.2	0.013	0.00002[c]
250—10/24/01	54	0.14	0.036	0.0031	0.0010	0.112	26.7	0.70	0.035	0.0007[c]	15.8	2.2	0.013	0.0030
250—10/25/01	54	NA	0.032	0.0035	0.0012	NA	28.8	NA	0.035	0.07	NA	NA	NA	NA
390—10/24/01	54	0.33	0.034	0.0127	0.0042	0.141	26.1	1.20	0.026	0.069	15.4	2.3	0.012	<0.0001
550—10/25/01	54	0.17	0.030	0.0112	0.0037	0.103	26.3	1.00	0.016	0.0540	14.7	2.3	0.011	0.0002[c]
648—10/25/01	48	0.26	0.035	0.0051	0.0017	0.109	26.7	1.30	0.041	0.0058	14.9	2.2	0.002	0.0003[c]
Outlet—11/07/01	43.0	NA	0.029	0.0035	0.0012	0.121	28.9	0.50 (0.433)	0.007	<0.011	14.4	2.0	0.011	<0.0001
Avg		0.24	0.032	0.0048	0.0016	0.117	27.8	0.92	0.049	0.037	14.7	2.1	0.012	0.00008

[a] Quantification limits: DOC, 0.04 mM; TOC, 0.04 mM; acetate, 0.002 mM; formate, 0.002 mM; propionate, 0.001 mM; DIC, 0.04 mM; Cl^-, 0.003 mM; HS^-, 0.0004 mM; SO_4^{2-}, 0.001; NH_4^+, 0.011 mM; Na, 0.004 mM; Ca, 0.001 mM; Mg, 0.002 mM; Fe, 0.0009 mM. TOC and DOC agree within the error. NA, not analyzed. NO_3^- and PO_4^{2-} were at or below the quantification limits (0.002 and 0.00005 mM, respectively) for all samples.

[b] HS^- was determined by two different protocols, gravimetric measurement and measurement of Zn by IPC-AES after precipitation with ZnCl (values in parentheses) (see Materials and Methods).

[c] Below the high-confidence quantification limit, but detectable.

some samples from the bailer (anions, cations, DIC, NH_3, and HPO_4^{2-}) were present in reduced amounts.

On-site measurements. Conductivity, pH, temperature, and E_h were measured at the borehole outlet with hand-held probes (HI98130 and HI98201; Hanna Instruments, Woonsocket, RI). Samples were verified as anaerobic with Chemets dissolved O_2 kits (0.1 to 1 ppm [0.03 to 0.3 mM] K-7501; Chemetrics, Inc., Calverton, VA). Downhole temperatures were obtained by attaching eight-point temperature labels (range, 37 to 65°C; EW-08068-20; Cole Parmer) to the bailer. These strips were certified accurate to ±3% by the manufacturer and agreed to within ±1°C with meter and glass thermometer readings at the outlet.

Laboratory procedures. Anions and organic acids were measured by ion chromatography (DX-320; Dionex, Sunnyvale, CA). The HPO_4^{2-} concentrations were determined using the MAGIC method (11). Cations were measured by inductively coupled plasma-atomic emission spectroscopy (ICP-AES) (ICP 4300 DV Optima; Perkin-Elmer, Wellesley, MA). NH_4^+ concentrations were determined by nesslerization (22). The HS^- contents were determined by two methods. For some samples (Table 1), HS^- was measured by filtering the ZnS precipitate from the water, dissolving it with 0.1 M HCl, and measuring the Zn content by ICP-AES. Alternatively, HS^- was determined gravimetrically from the ZnS precipitate in the samples for which the δ-^{34}S content was determined. The nonpurgeable TOC and DOC were measured from the acidified samples as CO_2 generated by catalytic combustion (EPA method 415.1), using an infrared detector (Tekmar Dohrman DC-190). For DOC, the sample was centrifuged at $10{,}000 \times g$ for 10 min, and the supernatant was analyzed. DIC was determined by adding phosphoric acid to the sealed serum vials, purging the samples with high-purity N_2, and measuring the CO_2 gas concentration by infrared absorption (LI-6252; LiCOR Biosciences, Lincoln, NE).

For sulfur isotope analyses, ZnS precipitates were rinsed, dried, and stored in baked glass vials at 60°C, and remaining water was acidified with HNO_3 to a pH of <5. About 5 ml of 0.4 M $BaCl_2$ was added to 60 ml of acidic solution, and samples were heated to 90°C on a hot plate for 3 h to precipitate $BaSO_4$. Both ZnS and $BaSO_4$ were converted to SO_2 in a Carlo Erba model 1100 elemental analyzer and analyzed by isotope ratio mass spectrometry, but the SO_4^{2-} concentrations were too low for accurate isotopic determinations. The $HgCl_2$-preserved water sample was acidified with phosphoric acid and analyzed by isotope ratio mass spectrometry (Rocky Mountain Instrumental Laboratories, Fort Collins, CO).

The dissolved gases were analyzed with a Kappa-5 reduced gas analyzer (RGA 5; Trace Analytical, Sparks, MD) equipped with a flame ionization detector (FID) and a Hg vapor detector (for H_2, CO, and CH_4). Gas separation occurred on individual columns for the RGA and FID, and the high-purity N_2 carrier gas flow rate was 40 ml min^{-1}. Compositional analyses of gas samples were performed at the Stable Isotope Laboratory at the University of Toronto as described by Ward et al. (74). Dissolved gas concentrations were derived from the gas volume abundance, the ratio of water to gas flow rates, and Henry's law constants following the procedure of Andrews and Wilson (2). Losses during retrieval caused dissolved gas concentrations to be lower in the bailer samples than in the packed outlet sample (Table 2). For this reason, the packed sample values were used for thermodynamic calculations. Because the measured gas concentrations may be underestimates due to phase separation at depth within the partially depressurized fault zone (41), they are considered minimum estimates. The δ^2H and $\delta^{18}O$ for three samples were also determined, using the procedures of Ward et al. (74).

Thermodynamic modeling. Measured substrate and product concentrations, Geochemist's Workbench (GWB 4.0.3; Rockware Inc., Golden, CO), and the database of Wolery et al. (18) were used for calculating speciation and the free energy for redox reactions. To relate the free energy of microbial redox reactions to microbial activity or ATP production, three assumptions were made. The first was that the conservation of energy during anaerobic electron transport processes (72) occurs for all of the metabolic processes involving the redox reactions that were considered. Secondly, a microorganism requires a minimum free energy charge (ΔG) of about -20 kJ mol^{-1} to capture energy from a given reaction (63), although microbial activity has been shown to proceed in the lab at -5 to -15 kJ mol^{-1} with syntrophic microbial consortia (28, 33, 64). Finally, the maximum rate at which this energy could be accrued was set by the rate of diffusion of the rate-limiting reactant to the microorganism (50). This rate (mol $cell^{-1}$ s^{-1}) is approximated by $4\pi DrC$, where C is the concentration of the rate-limiting reactant (mol kg^{-1}), D is the diffusivity of the reactant (cm^2 s^{-1}), and r is the radius of the microorganism (determined by flow cytometry). The reactant diffusivity increases with temperature according to the Stokes-Einstein relationship, and the values used were from the work of Cussler (17). This assumption presumes that deep subsurface microorganisms are nonmotile, which is likely given their extraordinarily low rates of growth (36, 58). The free energy flux (J $cell^{-1}$ s^{-1}) for a specific microbial redox reaction is equal to $4\pi DrC\Delta G$. The rate needs to be at least equivalent to the microorganism's maintenance energy demand in order for the pathway to be viable. In the case of a mesophilic nitrifying bacterium, for example, this maintenance demand is on the order of 10^{-16} J $cell^{-1}$ s^{-1} (71).

Flow cytometry. Samples were preserved in the field with 3.7% formaldehyde. The concentration and distribution of fluorescing particles and forward scatter and side scatter versus fluorescence intensity plots were determined on a FACScan flow cytometer (Becton Dickinson Inc., San Jose, CA). An internal standard consisting of 10 μl of 1.0-μm carboxylate-modified TransFluorSpheres (Molecular Probes, Eugene, OR) at 1.8×10^5 spheres μl^{-1} was added to 1 ml of sample. Samples were treated with the fluorescent nucleic acid dye SYTO13 (Molecular Probes) at 5 nM. Untreated aliquots of each sample were run to correct for autofluorescence. The average particle sizes in different areas of the plots were estimated for both treated and untreated parameters using Cell Quest software, and cell numbers were determined by the differences between the treated and untreated analyses. The average cell size was estimated by comparison with singlet and doublet clusters of the fluorescent spheres.

TABLE 2. Gas concentrations and stable isotope analyses

Sample	Gas concn (μM)[b]			Concn of isotope[b]										
	H_2	CH_4	CO[a]	$\delta^{34}S$ S^{2-}	$\delta^{34}S$ SO_4^{2-}	$\delta^{2}H$ H_2O	$\delta^{18}O$ H_2O	$\delta^{13}C$ DIC	$\delta^{13}C$ CH_4	$\delta^{2}H$ CH_4	$\delta^{2}H$ H_2	$\delta^{13}C$ C_2H_6	$\delta^{2}H$ C_2H_6	$\delta^{13}C$ C_3H_8
Outlet-083001	NA	NA	NA	11.8	<DL	−27.9	−5.0	−18.3	NA	NA	NA	NA	NA	NA
Outlet-091501	NA	NA	NA	NA	<DL	NA	NA	NA	NA	NA	NA	NA	NA	NA
Outlet-102401	NA	NA	NA	11.8	<DL	NA	NA	NA	NA	NA	NA	NA	NA	NA
125m-102401	0.16	2,110	32.1	12.7	<DL	NA	NA	−15.8	NA	NA	NA	NA	NA	NA
125m-102501	NA	NA	NA	NA	<DL	NA	NA	NA	−41.2	−369	<DL	−43.3	−222	<DL
250m-102401	NA	NA	NA	12.3	<DL	NA	NA	−16.3	−39.5	−323	<DL	−43.3	−261	<DL
250m-102501	0.81	4,740	8.6	NA	<DL	NA	NA	NA	NA	NA	NA	NA	NA	NA
390m-102401	NA	NA	NA	12.3	<DL	NA	NA	−15.5	−42.2	−346	<DL	−43.6	−292	<DL
550m-102501	NA	NA	NA	12.0	<DL	NA	NA	−15.6	−40.2	−370	<DL	−43.7	−297	−43.5
648m-102501	NA	NA	NA	12.7	<DL	NA	NA	−13.7	−40.9	−371	<DL	−44.0	−234	−42.9
Outlet-110701[c]	165	17,500	NA	11.6	<DL	−26.9	−5.6	−16.0	−40.2	−368	−685[d]	−43.1	−290	−42.0

[a] Measured only in the bailer samples.
[b] NA, not analyzed; DL, detection limit.
[c] C_2H_4, C_3H_8, C_4H_{10}, He, and N_2 were detected in the D8A Outlet-110701 sample at 732, 73, 1, 330, and 2,670 μM, respectively. O_2 was below the detection limit for all samples.
[d] Compared to standard mean ocean water.

Microscopy. Samples for electron microscopy were collected in 2-ml cryovials and fixed in the field with 2% (vol/vol) glutaraldehyde. One hundred microliters of each sample was suspended in 5 ml of filtered (0.2 μm) deionized water (Barnstead E-pure) and passed through a 13-mm, 0.4-μm-pore-size Isopore membrane filter (Millipore). Samples were processed through an ethanol dehydration series (25%, 50%, 75%, 100%, and 100% [30 min each]), followed by critical point drying using a Samdri PVT 3B CPD apparatus (Tousimis Research Corp.). Gold-coated samples were examined using a Hitachi S-4500 field emission scanning electron microscope (SEM) equipped with an EDAX system at an accelerating voltage of 10 kV with a 15-mm working distance. A total of 771 and 1,606 cells were counted from the 125-m and 250-m samples, using fluorescence in situ hybridization (FISH) analysis according to the procedure of Baker et al. (3), with EUB338 and ARC915 probes.

PLFA analysis. For phospholipid fatty acid (PLFA) analysis, biomasses from 8 liters of the outlet sample and 140 ml of the bailer samples were collected on Anodisc filters (0.2 μm by 47 or 25 mm; Laguna Niguel) (47). Compositional analyses of PLFAs were performed using procedures described by White and Ringelberg (75). Approximate bacterial cell densities were calculated using a conversion factor of 2.5×10^4 cells $pmol^{-1}$ PLFA (5).

Molecular analyses. Biomasses from 7 liters of sample D8A-Outlet-110701 and 140-ml bailer samples from 390, 550, and 648 m downhole were collected and preserved as previously described (46, 47). Filters were frozen at −20°C in the field, transported on dry ice, and stored at −80°C. DNA was extracted using an UltraClean Soil DNA mega prep kit (MoBio Laboratories, Solana Beach, CA), with shaking at 70°C and vortexing with beads. Final extracts (6 ml) were concentrated by precipitation in isopropanol-sodium acetate (9:1), followed by a 70% ethanol wash and suspension in 25 μl 10 mM Tris, 0.1 mM EDTA (47).

16S rRNA genes were amplified using La *Taq* polymerase (Takara Mirus Bio, Madison, WI) and primers at 0.2 μM. To remove possible contamination prior to template addition, digestion with HaeIII (0.1 units) was performed (incubation at 37°C for 20 min, followed by inactivation at 80°C for 25 min). One microliter of environmental DNA extract was added, and the reaction was incubated at 95°C for 5 min (1 cycle); at 95°C for 30 s, 50°C for 1 min, and 72°C for 1 min 30 s (35 cycles); and at 72°C for 20 min (1 cycle). Products were purified using UltraClean PCR clean-up kits (MoBio). Bacterial 16S rRNA genes were amplified using the primers 27f (10) and 1492R (39). Possibly due to the poor DNA extraction efficiency resulting from the gentle lysis procedure, reliable amplification of archaeal rRNA genes required a half-nested reaction in which the product generated using primers 21F (19) and 1492R (39) was used as the template for a second round of PCR with primers 21F and 958R (19). 16S rRNA gene cloning was done with TA cloning kits (Invitrogen). For each clone library, inserts were amplified from 96 clones, and the resulting products were screened by restriction fragment length polymorphism (RFLP) analysis. Representatives of each identified ribotype were purified using UltraClean PCR clean-up kits and then sequenced directly with vector primers (Big Dye reaction kit and ABI 3100 DNA sequencer; PE Applied Biosystems).

Chimeric sequences were identified using Bellerophon (29) and RDP Chimera-Check (13). The closest available matches to nonchimeric sequences were identified using the NCBI BLAST search tool (1). Sequences were managed within ARB (http://www.arb-home.de) and aligned with an ARB database built upon the 2002 Hugenholtz RDP alignment, using version 3.01 within the ARB_EDIT_4.1 tool followed by manual adjustments. Clone types (99% similarity) were designated after the alignment of sequences with ARB and comparisons of unambiguously aligned positions, as determined using the Lane mask (39). Maximum likelihood trees were generated using the Phylip FastDnaMl algorithm. Parsimony analysis and the calculation of bootstrap probabilities were performed with PAUP (Sinauer and Associates, Sunderland, MA). Phylogenetic trees based on Bayesian inferences were generated using MRBAYES (30), with 100,000 generations using a gamma rate correction, a sampling frequency of 100, and a burn-in value set to omit the first 350 trees from the consensus.

Terminal restriction fragment length polymorphism (T-RFLP) analysis of community 16S rRNA sequences was performed as previously described (47). To relate individual T-RFs to library clones, the 16S rRNA clone sequences were digested in silico, and the predicted T-RFs were compared to those produced by T-RFLP using an empirically derived accuracy criterion (47).

Functional genes were amplified using the same reagents as those used for 16S rRNA genes. The gene encoding the α subunit of methyl coenzyme M reductase (*mcrA*) was amplified from the 648-m sample with the primers (ME1F and ME2R) and PCR conditions described by Hales et al. (26). The dissimilatory sulfite reductase gene (*dsrAB*) was amplified from the 550-m sample as described by Baker et al. (3). PCR products were gel purified and cloned using TOPO-TA kits (Invitrogen). From each of the libraries, 48 random clones were typed by RFLP analysis. Clones were aligned with published representative sequences using Clustal X and imported into ARB, where neighbor-joining trees (10,000 bootstraps) were constructed. *dsrAB* sequences were imported into ARB, and phylogeny was generated using maximum likelihood. Bootstrap values and Bayesian inferences were also used to statistically support the nodes.

RESULTS AND DISCUSSION

The average pH and chlorinity were 9.1 and 32 mM, respectively, over the 70-day observation interval, and the E_h was −280 mV, equivalent to a pE of −1.4. The dissolved O_2 was below detection (<30 μM). The temperature at the outlet was 43.3°C, but increased to a maximum of 54°C at 250- to 550-m depths (Table 1).

Water age and source. Isotopically, the water in borehole D8A is meteoric in origin but distinct from that of the overlying dolomite (Table 2; Fig. 2). The δ^2H versus $\delta^{18}O$ measurements agreed with those for fracture water from nearby 4 Shaft of Kloof mine F3, as reported by Takai et al. (70), for which an age of 3 to 30 Ma was determined (41). Because the average

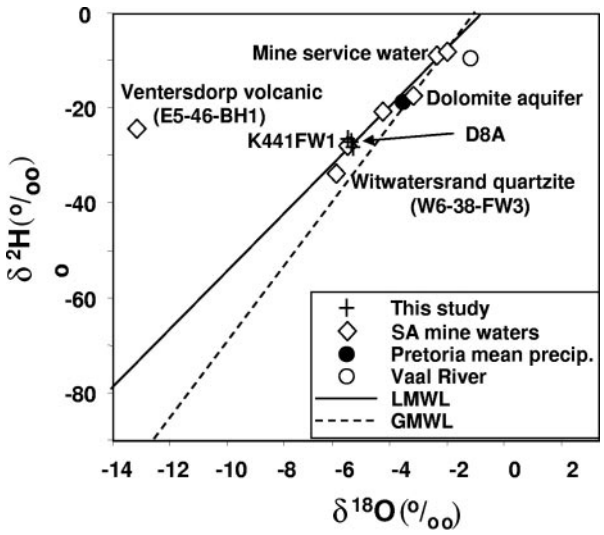

FIG. 2. δ^2H versus $\delta^{18}O$ plot showing positions of three samples from borehole D8A (crosses) in relation to other samples from nearby mines (diamonds) (41), Vaal River water (open circle) (21), and Pretoria annual average precipitation (closed circle) (31). The local mean water line (LMWL) is depicted as a solid line (44), and the global mean water line (GMWL) is shown as a dashed line (16). The samples from D8A occupy the same positions as those from the Kloof Mine sample, for which an age of 3 to 30 Ma was determined (K4-41-FW1) (41). A sample from the Witwatersrand supergroup quartzite (W6-38-FW3) (41) also plots very close to the samples from borehole D8A, whereas samples from the overlying dolomite aquifer, mine service water (51), and a Ventersdorp supergroup metavolcanic sample (E5-46-bh1) (47) occupy different positions. The figure is based on the work of Lippmann et al. (41), with permission.

chlorinity of D8A water also matched that of the Kloof sample (27.8 mM) (41) but the He concentration in D8A was four times greater that in the Kloof borehole water, at 1.3 mM (not shown) versus 0.3 mM (41), the age of D8A water is greater than that of water from the Kloof borehole. Using the models of Lippmann et al. (41), the estimated age is 4 (U = 240 ppm) to 53 Ma (U = 18 ppm), based on the flux and in situ He models, respectively.

The aqueous geochemistry most closely resembled that of borehole water associated with the Witwatersrand supergroup quartzite rather than that associated with the Ventersdorp supergroup metabasalt strata or the Chuniespoort dolomite. Most notably, the Ca^{2+}/Na^+ and Ca^{2+}/Mg^{2+} ratios of 0.14 and 180, respectively (Table 1), for D8A agree with the Ca^{2+}/Na^+ and Ca^{2+}/Mg^{2+} ratios of 0.07 and 333, respectively, for water from W6-38Bh-1 (Fig. 1), a Witwatersrand supergroup borehole (4), but not with the Ca^{2+}/Na^+ and Ca^{2+}/Mg^{2+} ratios of 0.4 and 2.060, respectively, for water from E5-46-Bh1 (Fig. 1), a Ventersdorp supergroup borehole (47), or the Ca^{2+}/Na^+ and Ca^{2+}/Mg^{2+} ratios of 2.1 and 1.1, respectively, for water from the Chuniespoort dolomite (52). The uniform geochemical signature along the depth profile (Table 1) also suggests that most of the borehole water originated from the deeper faults in the Witwatersrand quartzite.

The δ^2H value for H_2 (−685‰ VSMOW [Vienna Standard Mean Ocean Water]), relative to that for H_2O (−26.9‰ VSMOW) (Table 2), yielded an isotopic equilibration temperature of 60.5°C (8, 43), which is significantly greater than the 54°C measured downhole (Table 1). Based upon heat flow measurements obtained from West Witwatersrand line quartzite (49 ± 3 mW m^{-2}) (34) and a one-dimensional thermal conductivity model (49), this temperature constrains the water source to between 3.8 and 5.0 kmbls. The $>2.8 \times 10^6$ liters expelled prior to sampling would fill the volume of a hypothetical fracture with an average width of 0.5 cm and an area approximated by a plane of 250 by 2,035 m, which is compatible with the estimated source depth of the fault water. The fact that neither surface nor mine water breakthrough had occurred indicates that D8A is linked to a voluminous, deep fracture system with minimal connection to shallower sources. A similar inference was reached for the 3.1-kmbls Kloof Mine shaft 4 borehole water (70), whose 60°C temperature, exceeding the predicted in situ rock temperature by ~14°C, was attributed to upward migration along interconnected fractures (49). Collectively, the aqueous geochemistry and isotopic data are best explained by a deep source of ancient meteoric water. Since the water bears no evidence of interaction with the Ventersdorp supergroup metabasalt, the flow path must be confined to the underlying Witwatersrand supergroup quartzite.

TABLE 3. Cell number estimates by flow cytometry and phospholipid fatty acid analysis

Sample	Total cells · ml^{-1} (flow cytometry)	Bacterial cells · ml^{-1} (PLFA)	% Bacteria (FISH)[a]
DR938 H3 Outlet-102401	4.9×10^4	2.04×10^4	NA
DR938 H3 125M-102501	2.2×10^4	2.08×10^4	91[b]
DR938 H3 250M-102401	2.1×10^4	1.33×10^4	90[c]
DR938 H3 390M-102401	2.0×10^5	8.16×10^3	NA
DR938 H3 550M-102501	1.3×10^6	5.84×10^3	NA
DR938 H3 648M-102501	1.4×10^6	5.64×10^3	NA

[a] NA, not analyzed.
[b] Seven hundred seventy-one cells were counted.
[c] One thousand six hundred six cells were counted.

Microbial abundance and community structure. PLFA analysis indicated a bacterial biomass ranging from $\sim 6 \times 10^3$ to $\sim 2 \times 10^4$ cells ml^{-1}, with a possible increase (about three times) at shallower depths (Table 3). Total microbial cell densities given by flow cytometry were $\sim 1 \times 10^4$ to 4×10^4 cells ml^{-1} for samples from the 250-m depth to the outlet but were ~50 times higher for the two deepest samples ($\sim 1 \times 10^6$ cells ml^{-1}) (Table 3). Since PLFA is a measure of bacterial biomass, the discrepancy between these methods probably reflects an enrichment of archaea in the deeper samples. FISH analyses of the 125-m and 250-m samples revealed that 9% and 10%, respectively, of the cells were filamentous archaea, with the remainder being rod-shaped bacteria (Table 3). This observation is consistent with the PLFA cell densities being slightly less than the flow cytometry cell densities. Flow cytometry also indicated that most of the observed increase in total cell counts with increased depths is attributable to weakly stained, large-diameter (2 to 11 μm) particles (data not shown). SEM observations indicated that these particles were comprised of Si and Fe mineral colloids with attached filamentous microbial cells (data not shown). This colloidal material was visually apparent as a darker cast in the deeper samples. It was impossible to obtain accurate FISH counts in the deeper samples due to interference by mineral colloids, but it was qualitatively appar-

TABLE 4. Clone library summary

Clone group[a]	T-RF (bp)	Accession no.	General phylogenetic position	% of clones[b]			
				Outlet	390 m	550 m	648 m
D8A-1	209	AY768821	Low-G+C, gram-positive *Desulfotomaculum*	36	NA	100	98
D8A-2	93	AY768822	Unresolved within low-G+C, gram-positive group	0	NA	0	1
D8A-3	239	AY768823	Unresolved within low-G+C, gram-positive group	1	NA	0	0
D8A-4	69	AY768824	*Betaproteobacteria*, *Comamonadaceae*	63	NA	0	0
D8A-5	69	AY768825	*Betaproteobacteria*, *Comamonadaceae*	0	NA	0	1
D8A-6	197	AY768826	*Euryarchaeota*, *Methanobacteriaceae*	0	NA	3	0
D8A-7	197	AY768827	*Euryarchaeota*, *Methanobacteriaceae*	86	NA	95	97
D8A-8	335	AY768828	*Euryarchaeota*, *Methanobacteriaceae*	14	NA	3	3
D8A-mcrA1	NA	AY768819	*Euryarchaeota*, *Methanobacteriaceae*	93.5	100	NA	100
D8A-mcrA2	NA	AY768820	*Euryarchaeota*, *Methanobacteriaceae*	6.5	0	NA	0
D8A-dsr1	NA	AY768818	Low-G+C, gram-positive *Desulfotomaculum*	NA	NA	100	NA

[a] Ninety-six clones were screened for each rRNA library, and 48 clones were screened for the *mcrA* and *dsrAB* libraries.
[b] NA, not analyzed.

ent that the filaments far outnumbered the rod-shaped bacterial cells that dominated the shallower samples.

PCR-amplified 16S rRNA genes included both bacterial and archaeal genes, and T-RFLP profiles for both were dominated by a single major peak at all depths (data not shown). The bacterial peak (209 bp) corresponded to the predicted T-RF for the most abundant clone type (D8A-1; 98 to 100% of clones) (Table 4). Type D8A-1 is within the low-G+C gram-positive family *Peptococcaceae* and is most closely related to clones previously detected in W6-38-Bh1 borehole water (Fig. 1 and 3A) (4). The phylogenetic placement of this clone type, closely associated with a cluster of cultivated *Desulfotomaculum* species, was supported by multiple tree topologies with high confidence and bootstrap levels (Fig. 3A). D8A-1 also bore 96% identity to 16S rRNA sequences from 64°C water emitted from a borehole penetrating 3.5 million-year-old, off-axis ocean crust (15). The major archaeal T-RFLP peak, at 197 bp, corresponded to the most abundant archaeal clone (D8A-7; 95 to 97% of clones) (Table 4). All three archaeal taxa in the clone libraries were within the family *Methanobacteriaceae* (Fig. 3A), and two of them were detected by T-RFLP analysis. Neither the *Methanobacteriaceae* clones nor the D8A-1 clone has been detected in service water at the Driefontein mine (52, 70).

A β-proteobacterium (type D8A-4, *Comamonadaceae* family) comprised 63% of the outlet clone library (Table 4; Fig. 3A). *Comamonas*-like rRNA sequences have been reported for aerobic mine service water (52). The other β-proteobacterial clone type, D8A-5, was associated with the Fe- and Mn-oxidizing genera *Leptothrix* and *Sphaerotilus* (Fig. 3A) and was most similar to a clone previously detected in the outlet of E5-46-bh1 (Fig. 1) (47). The proteobacteria, therefore, were probably colonists, exploiting the oxic/anoxic interface at the borehole outlet. The remaining bacterial clones, D8A-2 and D8A-3, branched deeply within the *Firmicutes*, with D8A-3 being most closely related to a clone from E5-46-bh1 that appeared only after mine air was excluded for 2 months, suggesting its endemicity (47). The dominance of *Firmicutes* among the bacterial community is consistent with the physiological adaptations of this group to high temperatures and high-pH environments (61).

Key functional genes presumed to be involved in the energy metabolism of *Desulfotomaculum* (the dissimilatory sulfite reductase gene, *dsrAB*, for SO_4^{2-} reduction) (73) and of *Methanobacteriaceae* (the methyl-coenzyme M reductase gene, *mcrA*, for methanogenesis) (26) were also detected. A single *dsrAB* clone type (Table 4; Fig. 3B), which was most closely affiliated with *Desulfotomaculum* spp., and two *mcrA* clone types (Table 4; Fig. 3C) from within the *Methanobacteriaceae* were identified, confirming the genomic potential for SO_4^{2-} reduction and methanogenesis.

The microbial community structure of D8A fault water is therefore populated by a very simple microbial community dominated by a single bacterium (probably a sulfate reducer) and several closely related methanogens. Whether the methanogens or sulfate reducers dominate the microbial community within the fault is impossible to ascertain, because the filamentous methanogens may have preferentially adhered to the mineral colloids that formed and then settled to the bottom of the borehole as the hot fracture water cooled upon its ascent to the borehole outlet. This phenomenon would have gone undetected if not for the depth profile results. Colloid formation in deep artesian boreholes may be a common occurrence that needs to be considered if the emanating fluids are to be used to quantify the microbial community structure, as they have been in previous reports (12, 15, 25, 47, 68).

Predicted in situ microbial reactions. No significant difference was observed between DOC and TOC values, nor did either exhibit any trend with the borehole depth (Table 1). Acetate was the most abundant organic acid, ranging from 0.013 to 0.040 mM. The $\delta^{13}C$ value for DIC ranged from −13.7 to −18.3‰ Vienna Pee Dee Belemnite, averaging −15.9‰, with the deepest samples showing the least isotopic depletion (Table 2). Dividing cells were not observed by SEM or FISH, suggesting that the microorganisms were not growing at the time of sampling. The mM HS^- versus μM SO_4^{2-} concentrations were uniform along the length of the borehole (Table 1), indicating that SO_4^{2-} reduction had occurred within the fault system rather than the borehole water column.

These observations, combined with the short residence time in the borehole (ca. 3.5 h), argue for a steady-state balance between the observed water chemistry and the microbial population structure within the source fault water. To determine if the calculated Gibbs free energy of reaction (ΔG) and the

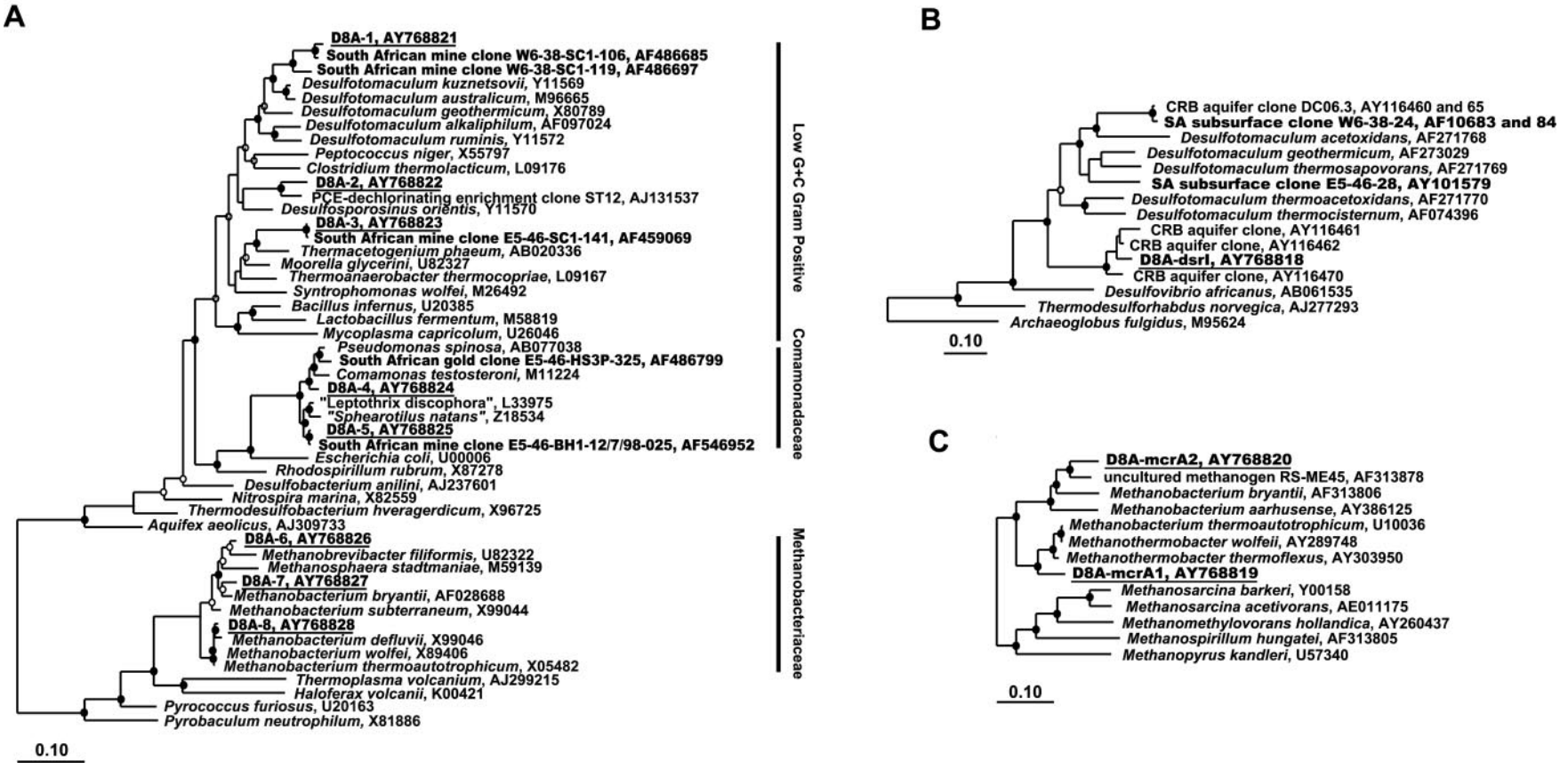

FIG. 3. Phylogenetic analyses. Clones from Driefontein Mine boreholes are depicted with bold lettering (47). Those specific for this study are underlined. (A) Phylogenetic dendrogram based on a maximum likelihood analysis (Phylip FastDnaMl) of 862 unambiguously aligned positions of 16S rRNA gene sequences. (B) Maximum likelihood tree of dissimilatory sulfite reductase (*dsrAB*) genes. (C) Phylogenetic tree based on neighbor-joining analyses of methyl-coenzyme M (*mcrA*) reductase gene sequences. Maximum likelihood tree topologies were compared against trees generated by Bayesian inferences and parsimony. Closed circles indicate nodes conserved in all three treatments, with Bayesian probability and parsimony bootstrap values of >75%. Nodes conserved in the majority of tree topologies and with 50 to 74% probabilities and bootstraps are designated by open circles. Branch points supported by fewer than two trees or having <50% probability and bootstrap values have no designation. In the neighbor-joining tree, branch points supported by >79% bootstrap values are designated by solid circles, those supported by 60 to 79% bootstrap values are designated with open circles, and those having bootstrap values of <60% are unlabeled. Bars, changes per nucleotide.

TABLE 5. Free energy and steady-state free energy flux for possible microbially mediated reactions[a]

Reaction no.	Redox reaction	Process	ΔG (kJ/mol) (43°C, pH 9.0)	ΔG (kJ/mol) (54°C, pH 9.0)	ΔG (kJ/mol) (61°C, pH 7.8)	FEF (kJ/cell-s) (43°C, pH 9.0)	FEF (kJ/cell-s) (54°C, pH 9.0)	FEF (kJ/cell-s) (61°C, pH 7.8)
1	$4CO + 5H_2O \rightarrow CH_4 + 3HCO_3^- + 3H^+$	Methanogenesis by CO disproportionation	−260	−257	−233	-8.6×10^{-14}	-9.8×10^{-14}	-1.0×10^{-13}
2	$4H_2 + H^+ + HCO_3^- \rightarrow CH_4 + 3H_2O$	Hydrogenotrophic methanogenesis	−70	−63	−68	-6.6×10^{-14}	-6.9×10^{-14}	-8.6×10^{-14}
3	$3H_2 + CO \rightarrow CH_4 + H_2O$	Hydrogenotrophic methanogenesis	−117	−113	−109	-3.9×10^{-14}	-4.3×10^{-14}	-4.9×10^{-14}
4	$4H_2 + H^+ + 2HCO_3^- \rightarrow$ acetate $+ 4H_2O$	Acetogenesis	−48	−41	−46	-3.9×10^{-14}	-3.8×10^{-14}	-5.0×10^{-14}
5	$4CO + SO_4^{2-} + 4H_2O \rightarrow 4HCO_3^- + HS^- + 3H^+$	Sulfate reduction	−297	−295	−271	-2.0×10^{-14}	-2.3×10^{-14}	-2.5×10^{-14}
6	$CO + 2H_2O \rightarrow HCO_3^- + H^+ + H_2$	Water-shift reaction	−47	−48	−41	-1.6×10^{-14}	-1.8×10^{-14}	-1.8×10^{-14}
7	$CO + H_2 \rightarrow 0.5$ acetate $+ 0.5H^+$	Acetogenesis	−72	−69	−64	-2.4×10^{-14}	-4.2×10^{-14}	-1.2×10^{-14}
8	$4H_2 + H^+ + SO_4^{2-} \rightarrow HS^- + 4H_2O$	Sulfate reduction	−107	−102	−107	-7.2×10^{-15}	-7.9×10^{-15}	-9.7×10^{-15}
9	Acetate $+ SO_4^{2-} \rightarrow 2HCO_3^- + HS^-$	Sulfate reduction	−59	−61	−61	-4.0×10^{-15}	-4.7×10^{-15}	-5.5×10^{-15}
10	Propane $+ 2.5SO_4^{2-} + 2H^+ \rightarrow 3HCO_3^- + 2.5H_2S + H_2O$	Sulfate reduction	−150	−153	−152	-4.0×10^{-15}	-4.8×10^{-15}	-5.5×10^{-15}
11	Acetate $+ H_2O \rightarrow CH_4 + HCO_3^-$	Acetoclastic methanogenesis	−22	−23	−23	-3.9×10^{-15}	-4.6×10^{-15}	-5.4×10^{-15}
12	Ethane $+ 1.75SO_4^{2-} + 1.5H^+ \rightarrow 2HCO_3^- + 1.75H_2S + H_2O$	Sulfate reduction	−97	−100	−99	-3.7×10^{-15}	-4.4×10^{-15}	-5.1×10^{-15}
13	$CH_4 + SO4^{2-} \rightarrow H_2O + HCO^{3-} + HS^-$	Anaerobic methane oxidation	−37	−38	−38	-2.5×10^{-15}	-3.0×10^{-15}	-3.5×10^{-15}

[a] FEF, free energy flux.

steady-state free energy flux favored SO_4^{2-} reduction and methanogenesis over other possible physiologies, calculations were performed using the borehole water chemistry for 83 possible microbial reactions at 43°C and 54°C and the measured outlet pH of 9.0. Calculations were also performed assuming a temperature of 61°C and a pH of 7.8, the predicted conditions for the fault water deduced from the borehole outlet pH and DIC after adjusting for the degassing of CO_2 within the borehole. The microbial reduction of Fe^{3+} was excluded due its reactivity at high levels of HS^-. The free energy flux calculations predicted that the three most thermodynamically favorable reactions were methanogenic (Table 5, reactions 1 to 3), with two reactions utilizing CO. Reactions 1 and 2 in Table 5 are known to be catalyzed by *Methanobacterium* spp. (69).

Three SO_4^{2-} reduction reactions (Table 5, reactions 8 to 10) were consistent with those known to be catalyzed by the genus *Desulfotomaculum*: they were the oxidation of H_2 (45, 48), the oxidation of acetate (65, 78), and the oxidation of propane (37). Although *Desulfotomaculum* spp. are not yet known to couple CO oxidation with SO_4^{2-} reduction (reaction 5) or to produce acetate from HCO_3^- or CO (reactions 4 and 7), they do possess the bifunctional and reversible CO dehydrogenase/acetyl-coenzyme A synthetase enzyme used for these metabolic processes and for reaction 9 (60, 77). Therefore, clone type D8A-1 might be expected to perform reaction(s) 4, 5, or 7. In hydrologically isolated systems, where cellular metabolism is slow and reactant concentrations change over geological time, the ability to exploit reversible pathways may be a critical survival adaptation.

Desulfotomaculum and *Methanobacterium* spp. are known to intimately interact during the transfer of H_2 and/or formate in thermophilic (55°C) anaerobic fermentation reactor biogranules utilizing low-molecular-weight, reduced organic compounds (32, 59). The high H_2 concentrations in the D8A water would seem to preclude this process, and cell assemblages, where low H_2 can be maintained in microsites by consumption rates that exceed diffusive flux, were not observed microscopically. Similarly, anaerobic CH_4 oxidation coupled to SO_4^{2-} reduction (Table 5, reaction 13) was less favorable than the individual methanogenic and SO_4^{2-}-reducing reactions. The $\delta^{13}C$ value for the ~121 μM DIC was greater than that for the mM CH_4, which would not be the case for anaerobic CH_4 oxidation by metabolic coupling between a SO_4^{2-} reducer and a methanogen. Furthermore, molecular evidence for predicted anaerobic CH_4 oxidizers (e.g., ANME-1) was not detected in either the 16S rRNA or *mcrA* clone library.

Microbial activity. The $\delta^{34}S_{sulfide}$ value was enriched in ^{34}S (average, 12.1‰ Cañon Diablo troilite [CDT]) (Table 2) relative to the sulfide value and more consistent with sulfate values that have been reported for the open borehole E5-46-Bh1 (i.e., $\delta^{34}S_{sulfide}$ = 1.4‰ CDT and $\delta^{34}S_{sulfate}$ = 19‰ CDT for E5-46-Bh1) (47). The sulfide isotopic enrichment and low SO_4^{2-} concentrations are consistent with microbially driven fractionation under SO_4^{2-} limitation, with minimal oxidation of the product sulfide. This is consistent with a hydrologically isolated environment and suggests that the microorganism represented by the D8A-1 clone performs sulfate reduction within the fault zone. The isotopically depleted $\delta^{13}C$ value for the DIC indicates that some of this sulfate reduction is tied to the oxidation of organic C, most likely acetate.

The $\delta^{13}C$ values for hydrocarbon gases trended towards greater depletion with increasing carbon chain lengths (C_1 versus $C_2 + C_3$), whereas the δ^2H became enriched from C_1 to C_2 (Table 2), both of which are indicative of abiogenic production (66, 74). If biological methanogenesis were occurring within the faults, then the concentrations of biogenic CH_4 would have to be >100 μM to isotopically shift the >17 mM abiogenic CH_4. The $\delta^{13}C$ value for the ~121 μM DIC is not as isotopically enriched as that reported by Stevens and McKinley for the Columbia River basalt aquifer (68), which suggests that autotrophically produced CH_4 would have to be <100 μM.

This ecosystem appears be controlled in a manner altogether different from that for subseafloor sediments (20, 55) and shallow terrestrial sedimentary environments, which are generally electron donor limited and represent the terminal portions of complex food webs which begin with detrital organic carbon and electron acceptors that are ultimately derived from the photosynthetically oxidizing surface world. In sediments, the H_2 concentration is controlled by the major terminal electron-accepting process, with methanogenesis and SO_4^{2-} reduction depleting H_2 to 7 to 10 and 1 to 1.5 nM, respectively (42). The D8A H_2 concentration is at least 3 orders of magnitude (Table 2) greater than would be predicted for either process. The potential cellular electron flux from H_2 is ~16 times that of SO_4^{2-}, but only about one-half that of HCO_3^-, taking into account the H^+ demands of the methanogenic reaction (Table 5). If the cellular HCO_3^- flux truly exceeds the H_2 flux, then this may explain why the $\delta^{13}C$ value for the DIC is not greatly isotopically enriched, since it is not limiting. The answer to why the autotrophic methanogens do not deplete the pool of H_2 may reside in the free energy for this reaction, which hovers between −63 and −70 kJ/mol (Table 5), close to the energy required for 1 mol of ATP. Significant reduction of the H_2 concentration in the presence of elevated CH_4 concentrations would reduce the free energy to below the minimum required for ATP production. The resulting H_2 concentration greatly exceeds the requirements imposed by the relatively miniscule SO_4^{2-} flux. The HCO_3^- concentration is controlled by the high Ca^{2+} concentration, high pH, high temperature, and solubility of calcite. This limitation on the electron acceptor flux and the minimal free energy requirement for methanogenesis may also account for the substantial excesses in H_2 that have been noted for other terrestrial subsurface environments (38, 68). Thus, given the H_2 abundance, both methanogenic and SO_4^{2-} reduction metabolisms can coexist.

The Columbia River basaltic aquifers are similar to the D8A fault water in that they are alkaline (7.9 to 9.9) and anaerobic, but they are also cooler (18 to 20°C), are much less saline (0.1 to 4 mM), contain much higher DIC concentrations (1 to 3 mM), are much less sulfidogenic (0.2 to 30 μM), and have much lower concentrations of CH_4 (2 to 209 μM). Rock/water microcosms incubated with a suite of well water samples under excess H_2 and CO_2 indicated that the balance between methanogens and SO_4^{2-} reducers was controlled by SO_4^{2-} concentrations, with methanogens dominating under conditions of SO_4^{2-} limitation (68). A subsequent quantitative rRNA analysis of the microbial community structure of some of the same wells (methanogenic [DB-11] and sulfidogenic [DC-06]) revealed that the active microbial community in the shallower methanogenic well was dominated by bacteria (64% bacteria versus 3% archaea) and that in the deeper sulfidogenic well was even more so (92% bacteria versus 1.8% archaea) (24). Gram-positive bacteria and δ-proteobacteria comprised a small portion of the bacterial component. Overall, the Columbia River basaltic aquifers represent a fresher, shallower, cooler, and microbially more diverse ecosystem than the deep faults intersected by D8A.

The D8A fault water ecosystem is also different in many respects from the 59°C, 70-m-deep groundwater of Lidy Hot Spring (12). The Lidy Spring water has a lower pH (6.9), lower salinity (0.2 mM), and much higher DIC (55 mM) and SO_4^{2-} (1.5 mM) concentrations than the D8A water. Its CH_4 concentration (0.1 mM), H_2 concentration (0.013 μM), and DOC concentration (20 μM) are much lower, making it an electron donor-limited environment, unlike D8A. The 16S rRNA gene library was almost entirely dominated (~99%) by methanogens (12), and sulfate reducers were not detected, despite the abundance of SO_4^{2-}.

The D8A results do bear a striking resemblance to those for the Lost City seafloor vent field, which has been interpreted as a microbial ecosystem driven by abiotic CH_4 and H_2 generation (7). The 60 to 75°C water venting from the Lost City carbonate towers (35) is similar to D8A borehole water in that it has a high pH (9 to 11), low DIC concentrations, high concentrations of abiogenic CH_4 (1 to 2 mM), and elevated H_2 concentrations (<1 to 15 mM) but differs by having a greater salinity and higher SO_4^{2-} concentrations (1 to 4 mM). The high-temperature microbial community is dominated by a methanogen, *Methanosarcinales*, and by thermophilic, sulfate-reducing *Firmicutes* (35), similar to D8A. Unlike the case for Lost City, however, in D8A the H_2 and possibly the SO_4^{2-} are generated by radiolysis of water in pyrite-rich quartzite (40), and the formation of abiogenic hydrocarbons occurs in the absence of ultramafic rock strata (67).

The identification of ocean vent microorganisms in the boreholes of deep South African Au mines has been reported previously, e.g., *Pyrococcus abysii* was reported by Takai et al. (70). In this study, the microbial ecosystem of D8A is most similar to that associated with off-axis ocean crust fluids and vents that form when seawater circulates through the ocean crust a few million years after it has moved from the axis and cooled. These thermophilic microorganisms could be inhabitants of the deep ocean selectively colonizing the ocean crust during the infiltration of SO_4^{2-}-rich seawater as part of hydrothermal circulation, or they may be permanent residents of the off-axis ocean crust with its unique thermal alkaline environment that are migrating horizontally as the ocean crust slowly moves away from the central axis.

The quartzite of the Witwatersrand Basin experienced sterilizing temperatures long after the last tectonic/metamorphic episode at 2 Ga. At 90 Ma, ~2 kilometers of the overlying Karoo supergroup sediments and volcanics was removed by erosion, and the underlying strata present at 3.2 kmbls began to cool from 120°C, reaching the present-day temperature at about 35 Ma (49). The 4- to 53-Ma He model ages for the fault water overlap with this post-Mesozoic uplift and cooling interval and are consistent with two origins for the microbial inhabitants of the D8A faults. They either existed in the overlying aquifers and selectively colonized the fault zone during meteoric water infiltration, or they have been residents of the ther-

mophilic, alkaline environment of the Witwatersrand subsurface and have slowly migrated downwards through the crust with uplift and cooling. Regardless of the origin of the D8A microbial community, oceanic and continental crusts with distinct thermal histories appear to host geochemically and microbially similar ecosystems. The Lost City hydrothermal field has been advanced as an exciting natural laboratory for the study of ecosystems driven by abiotic CH_4 and H_2 (7). The functionally analogous system described here significantly expands this concept to include an alternative mechanism for abiotic CH_4 and H_2 production within metamorphic and sedimentary strata of the continental deep subsurface.

ACKNOWLEDGMENTS

This research was supported by grants to T.C.O. from the NSF LExEn program (EAR-9714214) and to L.M.P. from the NASA Astrobiology Institute (NASA NNA04CC03A). SEM was performed at Surface Science Western, University of Western Ontario.

We gratefully acknowledge the support of Gold Fields Ltd., Driefontein Consolidated Mine, the Universities of Witwatersrand and Orange Free State, and Rob Wilson and colleagues of Turgis Technology (Pty.) Ltd. Special thanks to Dawie Nel, the Driefontein senior geologist, and Ben Kotze, the 9 Shaft master shaft sinker. Finally, we acknowledge the insightful comments of the reviewers, which greatly improved our interpretations of the data.

REFERENCES

1. **Altschul, S. F., T. L. Madden, A. A. Schaffer, J. H. Zhang, Z. Zhang, W. Miller, and D. J. Lipman.** 1997. Gapped BLAST and PSI-BLAST: a new generation of protein database search programs. Nucleic Acids Res. **25:** 3389–3402.
2. **Andrews, J. N., and G. B. Wilson.** 1987. The composition of dissolved gases in deep groundwater and groundwater degassing. Special paper 33. Geological Association of Canada, St. John's, Newfoundland, Canada.
3. **Baker, B. J., P. Hugenholtz, S. C. Dawson, and J. F. Banfield.** 2003. Extremely acidophilic protists from acid mine drainage host *Rickettsiales*-lineage endosymbionts that have intervening sequences in their 16S rRNA genes. Appl. Environ. Microbiol. **69:**5512–5518.
4. **Baker, B. J., D. P. Moser, B. J. MacGregor, S. Fishbain, M. Wagner, N. K. Fry, B. Jackson, N. Speolstra, S. Loos, K. Takai, B. S. Lollar, J. Fredrickson, D. Balkwill, T. C. Onstott, C. F. Wimpee, and D. A. Stahl.** 2003. Related assemblages of sulphate-reducing bacteria associated with ultradeep gold mines of South Africa and deep basalt aquifers of Washington State. Environ. Microbiol. **5:**267–277.
5. **Balkwill, D. L., F. R. Leach, J. T. Wilson, J. F. Mcnabb, and D. C. White.** 1988. Equivalence of microbial biomass measures based on membrane lipid and cell-wall components, adenosine-triphosphate, and direct counts in subsurface aquifer sediments. Microb. Ecol. **16:**73–84.
6. **Berner, E. K., and R. A. Berner.** 1987. The global water cycle. Prentice-Hall, Englewood Cliffs, N.J.
7. **Boetius, A.** 2005. Lost city life. Science **307:**1420–1422.
8. **Bottinga, Y.** 1969. Calculated fractionation factors for carbon and hydrogen isotope exchange in the system calcite-CO_2-graphite-methane-hydrogen and water vapour. Geochim. Cosmochim. Acta **33:**49–64.
9. **Brack, A.** 1993. Liquid water and the origin of life. Orig. Life Evol. Biosphere **23:**3–10.
10. **Braker, G., H. L. Ayala-del-Rio, A. H. Devol, A. Fesefeldt, and J. M. Tiedje.** 2001. Community structure of denitrifiers, bacteria, and archaea along redox gradients in Pacific Northwest marine sediments by terminal restriction fragment length polymorphism analysis of amplified nitrite reductase (*nirS*) and 16S rRNA genes. Appl. Environ. Microbiol. **67:**1893–1901.
11. **Bulldis, A., and D. Karl.** 1998. Application of a novel method for phosphorus determinations in the oligotrophic North Pacific Ocean. Limnol. Oceanogr. **43:**1565–1577.
12. **Chapelle, F. H., K. O'Neill, P. M. Bradley, B. A. Methe, S. A. Ciufo, L. L. Knobel, and D. R. Lovley.** 2002. A hydrogen-based subsurface microbial community dominated by methanogens. Nature **415:**312–315.
13. **Cole, J. R., B. Chai, T. L. Marsh, R. J. Farris, Q. Wang, S. A. Kulam, S. Chandra, D. M. McGarrell, T. M. Schmidt, G. M. Garrity, and J. M. Tiedje.** 2003. The Ribosomal Database Project (RDP-II): previewing a new autoaligner that allows regular updates and the new prokaryotic taxonomy. Nucleic Acids Res. **31:**442–443.
14. **Colwell, F. S., T. C. Onstott, M. E. Delwiche, D. Chandler, J. K. Fredrickson, Q. J. Yao, J. P. McKinley, D. R. Boone, R. Griffiths, T. J. Phelps, D. Ringelberg, D. C. White, L. LaFreniere, D. Balkwill, R. M. Lehman, J. Konisky, and P. E. Long.** 1997. Microorganisms from deep, high temperature sandstones: constraints on microbial colonization. FEMS Microbiol. Rev. **20:**425–435.
15. **Cowen, J. P., S. J. Giovannoni, F. Kenig, H. P. Johnson, D. Butterfield, M. S. Rappe, M. Hutnak, and P. Lam.** 2003. Fluids from aging ocean crust that support microbial life. Science **299:**120–123.
16. **Craig, H.** 1961. Isotopic variations in meteoric waters. Science **133:**1702–1703.
17. **Cussler, E. L.** 1984. Diffusion mass transfer in fluid systems. Cambridge University Press, Cambridge, United Kingdom.
18. **Delany, J. M., and S. R. Lundeen.** 1990. The LLNL thermochemical database UCRL-21658. Lawrence Livermore National Laboratory, Livermore, Calif.
19. **DeLong, E. F.** 1992. Archaea in coastal marine environments. Proc. Natl. Acad. Sci. USA **89:**5685–5689.
20. **D'Hondt, S., B. B. Jorgensen, D. J. Miller, A. Batzke, R. Blake, B. A. Cragg, H. Cypionka, G. R. Dickens, T. Ferdelman, K. U. Hinrichs, N. G. Holm, R. Mitterer, A. Spivack, G. Z. Wang, B. Bekins, B. Engelen, K. Ford, G. Gettemy, S. D. Rutherford, H. Sass, C. G. Skilbeck, I. W. Aiello, G. Guerin, C. H. House, F. Inagaki, P. Meister, T. Naehr, S. Niitsuma, R. J. Parkes, A. Schippers, D. C. Smith, A. Teske, J. Wiegel, C. N. Padilla, and J. L. S. Acosta.** 2004. Distributions of microbial activities in deep subseafloor sediments. Science **306:**2216–2221.
21. **Duane, M. J., G. Pigozzi, and C. Harris.** 1997. Geochemistry of some deep gold mine waters from the western portion of the Witwatersrand Basin, South Africa. J. Afr. Earth Sci. **24:**105–123.
22. **Eaton, A. D., L. S. Clesceri, and A. E. Greenberg.** 1995. Standard methods for the examination of water and wastewater, 19th ed. American Public Health Association, Washington, D.C.
23. **Fredrickson, J. K., and T. C. Onstott.** 1996. Microbes deep inside the Earth. Sci. Am. **275:**68–73.
24. **Fry, N. K., J. K. Fredrickson, S. Fishbain, M. Wagner, and D. A. Stahl.** 1997. Population structure of microbial communities associated with two deep, anaerobic, alkaline aquifers. Appl. Environ. Microbiol. **63:**1498–1504.
25. **Gold, T.** 1992. The deep, hot biosphere. Proc. Natl. Acad. Sci. USA **89:**6045–6049.
26. **Hales, B. A., C. Edwards, D. A. Ritchie, G. Hall, R. W. Pickup, and J. R. Saunders.** 1996. Isolation and identification of methanogen-specific DNA from blanket bog peat by PCR amplification and sequence analysis. Appl. Environ. Microbiol. **62:**668–675.
27. **Haveman, S. A., K. Pedersen, and P. Ruotsalainen.** 1999. Distribution and metabolic diversity of microorganisms in deep igneous rock aquifers of Finland. Geomicrobiol. J. **16:**277–294.
28. **Hoehler, T. M., M. J. Alperin, D. B. Albert, and C. S. Martens.** 2001. Apparent minimum free energy requirements for methanogenic archaea and sulfate-reducing bacteria in an anoxic marine sediment. FEMS Microbiol. Ecol. **38:**33–41.
29. **Huber, T., G. Faulkner, and P. Hugenholtz.** 2004. Bellerophon: a program to detect chimeric sequences in multiple sequence alignments. Bioinformatics **20:**2317–2319.
30. **Huelsenbeck, J. P., and F. Ronquist.** 2001. MRBAYES: Bayesian inference of phylogenetic trees. Bioinformatics **17:**754–755.
31. **IAEA/WMO.** 2002. Global Network for Isotopes in Precipitation (GNIP) database. http://isohis.iaea.org.
32. **Imachi, H., Y. Sekiguchi, Y. Kamagata, A. Ohashi, and H. Harada.** 2000. Cultivation and in situ detection of a thermophilic bacterium capable of oxidizing propionate in syntrophic association with hydrogenotrophic methanogens in a thermophilic methanogenic granular sludge. Appl. Environ. Microbiol. **66:**3608–3615.
33. **Jackson, B. E., and M. J. McInerney.** 2002. Anaerobic microbial metabolism can proceed close to thermodynamic limits. Nature **415:**454–456.
34. **Jones, M. Q.** 1988. Heat flow in the Witwatersrand Basin and environs and its significance for the South African shield geotherm and lithosphere thickness. J. Geophys. Res. **93:**3243–3260.
35. **Kelley, D. S., J. A. Karson, G. L. Fruh-Green, D. R. Yoerger, T. M. Shank, D. A. Butterfield, J. M. Hayes, M. O. Schrenk, E. J. Olson, G. Proskurowski, M. Jakuba, A. Bradley, B. Larson, K. Ludwig, D. Glickson, K. Buckman, A. S. Bradley, W. J. Brazelton, K. Roe, M. J. Elend, A. Delacour, S. M. Bernasconi, M. D. Lilley, J. A. Baross, R. T. Summons, and S. P. Sylva.** 2005. A serpentinite-hosted ecosystem: the Lost City hydrothermal field. Science **307:**1428–1434.
36. **Kieft, T. L., and T. J. Phelps.** 1997. Life in the slow lane: activities of microorganisms in the subsurface, p. 137–164. *In* P. S. Amy and D. L. Haldeman (ed.), The microbiology of the terrestrial deep subsurface. CRC Lewis Publishers, Boca Raton, Fla.
37. **Kniemeyer, O., K. Knittel, S. Sievert, H. Wilkes, and F. Widdel.** 2003. Anaerobic degradation of propane and butane in enrichment cultures under sulfate-reducing conditions. American Society for Microbiology, Washington, D.C.
38. **Kotelnikova, S., and K. Pedersen.** 1998. Distribution and activity of meth-

anogens and homoacetogens in deep granitic aquifers at Aspo Hard Rock Laboratory, Sweden. FEMS Microbiol. Ecol. **26:**121–134.
39. **Lane, D. J.** 1991. 16S/23S rRNA sequencing, p. 115–175. *In* E. Stackebrandt and M. Goodfellow (ed.), Nucleic acid techniques in bacterial systematics. John Wiley and Sons, New York, N.Y.
40. **Lin, L.-H., J. A. Hall, J. Lippmann, J. A. Ward, B. Sherwood Lollar, and T. C. Onstott.** 2005. Radiolytic H_2 in the continental crust: nuclear power for deep subsurface microbial communities. Geochem. Geophys. Geosys. **6:**Q07003. [Online.] doi:10.1029/2004GC000907.
41. **Lippmann, J., M. Stute, T. Torgerson, D. P. Moser, J. Hall, L. Lin, M. Borcsik, R. E. S. Bellamy, and T. C. Onstott.** 2003. Dating ultra-deep mine waters with noble gases and ^{36}Cl, Witwatersrand Basin, South Africa. Geochim. Cosmochim. Acta **67:**4597–4619.
42. **Lovley, D. R., F. H. Chapelle, and J. C. Woodward.** 1994. Use of dissolved H_2 concentrations to determine distribution of microbially catalyzed redox reactions in anoxic groundwater. Environ. Sci. Technol. **28:**1205–1210.
43. **Majoube, M.** 1971. Fractionnement en oxygene-18 et en deuterium entre l'eau et sa vapeur. J. Chem. Phys. **197:**1423–1436.
44. **Mazor, E., and B. T. Verhagen.** 1983. Dissolved ions, stable and radioactive isotopes and noble gases in thermal water of South Africa. J. Hydrol. **63:** 315–329.
45. **Mori, K., M. Hatsu, R. Kimura, and K. Takamizawa.** 2000. Effect of heavy metals on the growth of a methanogen in pure culture and coculture with a sulfate-reducing bacterium. J. Biosci. Bioeng. **90:**260–265.
46. **Moser, D. P., H. W. Martin, and P. J. Boston.** 2002. Microbiological sampling in caves and mines, p. 821–835. *In* G. E. Bitton (ed.), Encyclopedia of environmental microbiology. John Wiley and Sons, Inc., New York, N.Y.
47. **Moser, D. P., T. C. Onstott, J. K. Fredrickson, F. J. Brockman, D. L. Balkwill, G. R. Drake, S. M. Pfiffner, D. C. White, K. Takai, L. M. Pratt, J. Fong, B. S. Lollar, G. Slater, T. J. Phelps, N. Spoelstra, M. Deflaun, G. Southam, A. T. Welty, B. J. Baker, and J. Hoek.** 2003. Temporal shifts in the geochemistry and microbial community structure of an ultradeep mine borehole following isolation. Geomicrobiol. J. **20:**517–548.
48. **Nilsen, R. K., T. Torsvik, and T. Lien.** 1996. *Desulfotomaculum thermocisternum* sp. nov., a sulfate reducer isolated from a hot North Sea oil reservoir. Int. J. Syst. Bacteriol. **46:**397–402.
49. **Omar, G. I., T. C. Onstott, and J. Hoek.** 2003. The origin of deep subsurface microbial communities in the Witwatersrand Basin, South Africa as deduced from apatite fission track analyses. Geofluids **3:**69–80.
50. **Onstott, T. C.** 2004. Impact of CO_2 injections on deep subsurface microbial ecosystems and potential ramifications for the surface biosphere, p. 1207–1239. *In* D. C. Thomas and S. M. Benson (ed.), The CO_2 capture and storage project, vol. II. Elsevier, New York, N.Y.
51. **Onstott, T. C., and B. Sherwood-Lollar.** Data not shown.
52. **Onstott, T. C., D. P. Moser, S. M. Pfiffner, J. K. Fredrickson, F. J. Brockman, T. J. Phelps, D. C. White, A. Peacock, D. Balkwill, R. Hoover, L. R. Krumholz, M. Borscik, T. L. Kieft, and R. Wilson.** 2003. Indigenous and contaminant microbes in ultradeep mines. Environ. Microbiol. **5:**1168–1191.
53. **Onstott, T. C., T. J. Phelps, F. S. Colwell, D. Ringelberg, D. C. White, D. R. Boone, J. P. McKinley, T. O. Stevens, D. L. Balkwill, T. Griffin, T. Kieft.** 1998. Observations pertaining to the origin and ecology of microorganisms recovered from the deep subsurface of Taylorsville Basin, Virginia. Geomicrobiol. J. **15:**353–385.
54. **Orphan, V. J., L. T. Taylor, D. Hafenbradl, and E. F. Delong.** 2000. Culture-dependent and culture-independent characterization of microbial assemblages associated with high-temperature petroleum reservoirs. Appl. Environ. Microbiol. **66:**700–711.
55. **Parkes, R. J., B. A. Cragg, and P. Wellsbury.** 1999. Recent studies on bacterial populations and processes in subseafloor sediments: a review. Hydrogeol. J. **8:**11–28.
56. **Pedersen, K.** 1997. Microbial life in deep granitic rock. FEMS Microbiol. Rev. **20:**399–414.
57. **Pedersen, K., L. Hallbeck, J. Arlinger, A. C. Erlandson, and N. Jahromi.** 1997. Investigation of the potential for microbial contamination of deep granitic aquifers during drilling using 16S rRNA gene sequencing and culturing methods. J. Microbiol. Methods **30:**179–192.
58. **Phelps, T. J., E. M. Murphy, S. M. Pfiffner, and D. C. White.** 1994. Comparison between geochemical and biological estimates of subsurface microbial activities. Microb. Ecol. **28:**335–349.
59. **Plugge, C. M., M. Balk, and A. J. M. Stams.** 2002. *Desulfotomaculum thermobenzoicum* subsp. *thermosyntrophicum* subsp. nov., a thermophilic, syntrophic, propionate-oxidizing, spore-forming bacterium. Int. J. Syst. Evol. Microbiol. **52:**391–399.
60. **Ragsdale, S. W., and M. Kumar.** 1996. Nickel-containing carbon monoxide dehydrogenase/acetyl-CoA synthase. Chem. Rev. **96:**2515–2539.
61. **Reysenbach, A.-L., D. Gotz, and D. Yernool.** 2002. Microbial diversity of marine and terrestrial thermal springs, p. 345–421. *In* J. T. Staley and A.-L. Reysenbach (ed.), Biodiversity of microbial life. Wiley-Liss, Inc., New York, N.Y.
62. **Robb, L. J., and F. M. Meyer.** 1995. The Witwatersrand Basin, South Africa: geological framework and mineralization processes. Ore Geol. Rev. **10:**67–94.
63. **Schink, B.** 1997. Energetics of syntrophic cooperation in methanogenic degradation. Microbiol. Mol. Biol. Rev. **61:**262–280.
64. **Scholten, J. C. M., and R. Conrad.** 2000. Energetics of syntrophic propionate oxidation in defined batch and chemostat cocultures. Appl. Environ. Microbiol. **66:**2934–2942.
65. **Scholten, J. C. M., and A. J. M. Stams.** 2000. Isolation and characterization of acetate-utilizing anaerobes from a freshwater sediment. Microb. Ecol. **40:**292–299.
66. **Sherwood-Lollar, B., T. D. Westgate, J. A. Ward, G. F. Slater, and G. Lacrampe-Couloumbe.** 2002. Abiogenic formation of alkanes in the Earth's crust as a minor source for global hydrocarbon reservoirs. Nature **416:**522–524.
67. **Sherwood Lollar, B., G. Lacrampe-Couloume, G. F. Slater, J. Ward, D. P. Moser, T. M. Gihring, L.-H. Lin, and T. C. Onstott.** Unravelling abiogenic and biogenic sources of methane in the Earth's deep subsurface. Chem. Geol., in press.
68. **Stevens, T. O., and J. P. McKinley.** 1995. Lithoautotrophic microbial ecosystems in deep basalt aquifers. Science **270:**450–454.
69. **Stupperich, E., K. E. Hammel, G. Fuchs, and R. K. Thauer.** 1983. Carbon-monoxide fixation into the carboxyl group of acetyl coenzyme-A during autotrophic growth of *Methanobacterium*. FEBS Lett. **152:**21–23.
70. **Takai, K., D. P. Moser, M. DeFlaun, T. C. Onstott, and J. K. Fredrickson.** 2001. Archaeal diversity in waters from deep South African gold mines. Appl. Environ. Microbiol. **67:**5750–5760.
71. **Tappe, W., A. Laverman, M. Bohland, M. Braster, S. Rittershaus, J. Groeneweg, and H. W. van Verseveld.** 1999. Maintenance energy demand and starvation recovery dynamics of *Nitrosomonas europaea* and *Nitrobacter winogradskyi* cultivated in a retentostat with complete biomass retention. Appl. Environ. Microbiol. **65:**2471–2477.
72. **Thauer, R. K., K. Jungermann, and K. Decker.** 1977. Energy conservation in chemotrophic anaerobic bacteria. Bacteriol. Rev. **41:**100–180.
73. **Wagner, M., A. J. Roger, G. A. Flax, G. A. Brusseau, and D. A. Stahl.** 1998. Phylogeny of dissimilatory sulfite reductases supports an early origin of sulfate respiration. J. Bacteriol. **180:**2975–2982.
74. **Ward, J. A., G. F. Slater, D. P. Moser, L. H. Lin, G. Lacrampe-Couloume, A. S. Bonin, M. Davidson, J. A. Hall, B. Mislowack, R. E. S. Bellamy, T. C. Onstott, and B. S. Lollar.** 2004. Microbial hydrocarbon gases in the Witwatersrand Basin, South Africa: implications for the deep biosphere. Geochim. Cosmochim. Acta **68:**3239–3250.
75. **White, D. C., and D. B. Ringelberg.** 1998. Signature lipid biomarker analysis, p. 255–272. *In* R. S. Burlage et al. (ed.), Techniques in microbial ecology. Oxford University Press, New York, N.Y.
76. **Whitman, W. B., D. C. Coleman, and W. J. Wiebe.** 1998. Prokaryotes: the unseen majority. Proc. Natl. Acad. Sci. USA **95:**6578–6583.
77. **Widdel, F.** 1988. Microbiology of sulfate- and sulfur-reducing bacteria, p. 469–585. *In* A. J. B. Zehnder (ed.), Biology of anaerobic microorganisms. Wiley and Sons, New York, N.Y.
78. **Widdel, F., and N. Pfennig.** 1977. A new anaerobic, sporing, acetate-oxidizing, sulfate-reducing bacterium, *Desulfotomaculum* (emend.) *acetoxidans*. Arch. Microbiol. **112:**119–122.